Volume 2 • Issue 1 • 2020

Research Article

Journal of Medicine and Surgical Sciences

A Novel Bioengineered Material to Reverse Intervertebral Disc Degeneration

Daisuke Fukui[1,2], Koichi Masuda[1], Michael Zimber[3], Stephanie Y. Adachi[1], Natsuko Arimoto[1], Jeong Ho Kim[3], Martin Latterich[3], Gail K. Naughton[3]*

[1]Department of Orthopaedic Surgery University of California, San Diego 9500 Gilman Drive La Jolla, CA 92093

[2]Department of Orthopaedic Surgery Wakayama Medical University 811-1 Kimiidera Wakayama City, Wakayama 641-8510 Japan

[3]Histogen, Inc. 10655 Sorrento Valley Road San Diego, CA 92121

***Corresponding Author:** Gail Naughton, Histogen, Inc. 10655 Sorrento Valley Road, San Diego, CA 92121, USA.

Received: March 31, 2020; **Published:** May 04, 2020

Abstract

Intervertebral disc degeneration (IDD) is a major cause of chronic and debilitating back pain whose prevalence and severity make it a major health issue of substantial socioeconomic importance. The prevalence of chronic disabling back pain has tripled over the last 20 years [1] and the treatment of lower back pain in the United States is estimated to cost more than $100 billion per year. [2] Current treatment options are mostly palliative since disc tissue has little intrinsic repair capacity once a matrix synthesis/degradation imbalance occurs. Our bioengineered naturally secreted compositions have demonstrated the ability to decrease/remove protease and inflammatory cytokine activity and stimulate native cells to secrete new matrix production in vitro, and to maintain nucleus hydration and help to recover from the initial disc height loss in the semi-acute rabbit annular puncture model.

Keywords: *Intervertebral disc; Cell conditioned medium; Disc degeneration; Tissue regeneration; Stem cell proliferation*

Abbreviations: Cell conditioned medium (CCM), human extracellular matrix (hECM), mesenchymal stem cell (MSC), intervertebral disc (IVD), intervertebral disc degeneration (IDD), annulus fibrosus (AF), nucleus pulposus (NP)

Introduction

Intervertebral discs (IVDs) are composed of an annulus fibrosus (AF) and a nucleus pulposus (NP). The AF encloses the NP and is a strong radial tire–like structure made up of concentric sheets of collagen fibers connected to the vertebral endplates. The sheets are orientated at various angles. Both the AF and NP are composed of water, collagen, and proteoglycans (PGs). The NP contains a hydrated gel–like matter that resists compression. In early disc degeneration, changes to the matrix of the NP and inner AF are believed to be a result of a shift in the balance of anabolic and catabolic activities to result in an increased proteolytic activity. [3,4,5] Research has shown that an onset of an inflammatory process plays a major role in mediating the matrix breakdown. [6,7] Disc cells are capable of producing several proinflammatory cytokines, such as interleukin (IL)-1, IL-4, IL-6, IL-8, IL-112, IL-17, interferon-γ, and tumor necrosis factor-α. [6,8,9,10,11] These cytokines mimic noxious effects [12,13] and are powerful direct stimuli of nociceptive triggers. [10,14] In addition, by-products of disc cell metabolism, such as lactic acid, may also be noxious. [15,16] It is believed that such noxious

stimuli irritate the nociceptive receptors in the outer AF and osseous endplates. Inner and outer AF cells produce proinflammatory cytokines IL-1 and TNF-α which have shown to be directly involved in pain signaling by sensitization. TNF-α has been shown to be higher and more strongly correlated to disc degeneration from symptomatic as compared to asymptomatic patients having similar amounts of degeneration. [17] In moderate to advanced intervertebral disc degeneration (IDD) a disorganization of the AF and general fibrosis of the NP occurs [18,19] which contribute to the AF becoming stiffer and weaker with age, [20] and the development of AF tears. [18]

IVDs contain very few cells embedded in a matrix rich in collagens, glycoproteins, and proteoglycans. In a healthy cells maintain and repair the matrix, however damaged IVDs have an imbalance between matrix synthesis and secretion. The degraded matrix can no longer carry the load effectively and the cells become necrotic as disc degeneration continues. Replacing the proper matrix composition while reducing inflammation and protease activity has the potential of reversing the disc degenerative process and regenerating a functional IVD.

Extracellular matrix composition: The collagen network is similar to that in hyaline cartilage and increases from the center of the NP to the outer AF, providing a network to support the cells and confine the proteoglycans. [21] Hydrated proteoglycans are immobilized within and inflate the collagen network. The AF contains collagen type I, II, III, V, VI, IX, XI and the NP contains type II, VI, IX, and XI. [22] The concentration of the proteoglycans in the IVD plays a major role in providing the correct mechanical properties and the hydrophilicity of the proteoglycans allows them to influence the collagen organization. The cells of the NP produce significantly more proteoglycans than in the AF, which are responsible for water attraction and retention and swelling. [22]

Cells represent only 1% of the IVD volume with chondrocyte-like cells in the NP, fibrocartilaginous cells in the inner AF, and fibroblast-like cells in the outer AF. [23] These cells are specialized chondrocytes modulated by the organization of their cytoskeleton and are responsible for all of the extracellular matrix molecules in the IVD. Mechanical stress, osmotic and ionic environment, and nutrient supply are the most important stimuli of matrix secretion. Nutrients are provided to the cells by a blood supply beneath the hyaline cartilage end plate while cell activity is regulated by growth factors and cytokines. As with hyaline cartilage of the joint, nutrient transport into and through the disc is largely due to diffusion with diffusion coefficients increasing in the NP. [24] The IVD cells are completely surrounded by a pericellular matrix (PCM) which contains collagen type IV, II and IX, aggrecan, hyaluronan, decorin, and fibronectin. [25,26,22] Treatments for IDD include intradiscal steroid injections to reduce inflammation none of which have been associated with prolonged pain relief and fusion and removal can have significant complications associated with them. [26] Our plan is to use soluble (CCM) and insoluble proteins (hECM) secreted by hypoxia-induced stem cells to reduce or eliminate the inflammation associated with IDD and induce disc regeneration.

Histogen has developed a cell conditioned media (CCM) and a naturally secreted extracellular matrix (hECM) that are very embryonic in composition and have been shown to stimulate stem cells in vivo. In contrast to adults, fetal mammals are capable of regenerating injured tissues without scarring during the first two trimesters of gestation. [27,28] The scar-less healing phenomenon is associated with hypoxia (1-5% oxygen), low levels of TGFβ and FGF, and a predominance of collagens III and V. [29] The mechanism of fetal scar-less regeneration and the embryogenetic mechanisms of chondrogenesis is still not fully understood, [30,31] but a deeper understanding of how recapitulating the embryonic mechanism in the treatment of disc degeneration may offer tremendous benefit in reversing the pathogenesis of this disease. Recent research utilizing gene expression analysis to compare fetal and adult genes and their implied protein regulation in response to tissue injury has shown that the most relevant events involved proteins associated with the immune response and inflammation and proteins involved in cell growth and proliferation and cartilage tissue and development. [32] Proteins associated with the inflammatory process were found to be significantly upregulated following injury in adults but not in fetal animals; proteoglycans were upregulated only in fetal sheep post cartilage injury.

Neonatal fibroblasts are grown under hypoxia (3-5% oxygen) and suspension culture to mimic the embryonic environment. During this culture process the fibroblasts revert back to multipotent stem cells, as evidenced by the up-regulation of pluripotent stem cell-associated genes that include, SOX2, OCT4/POU5F1, NANOG and KLF4, and by the expression of stem cell-associated proteins, including nodal, brachyury, nestin and Oct4. [33,34] The CCM harvested during the manufacturing process and the hECM harvested

at the conclusion of the process have the potential of reducing inflammation and stimulating autologous IVD cells, which can lead to the repair of IVD matrix.

Our in vitro studies demonstrated that the CCM and hECM individually support the regulation and proliferation of human mesenchymal stem cells (hMSCs), as well as cell surface markers, showing the maintenance of stemness and inducing the upregulation of aggrecan and Collagen II. [33] These are all important components in hyaline and hyaline-like cartilage matrix regeneration which would be critical in reversing IVD degeneration and reestablishing the natural mechanical strength of the IVD. Additional studies were performed to help analyze the CCM and hECM components and their in vitro, ex vivo, and in vivo influence on chondrocytes as well as other IVD cells.

Materials and Methods or Experimental Procedures

Production of CCM: Human neonatal fibroblasts were seeded on dextran beads and grown in a computer-controlled closed 10L bioreactor under 3-5% oxygen. Cells were fed a serum free media daily through a perfusion system. Once cells reached confluence the CCM was removed daily for up to twelve weeks, concentrated through a 10kD filter, and clarified.

Production of hECM: At the end of the 3-month culture period, the insoluble material consisting of microcarrier beads, cells and deposited ECM was collected, washed in sterile distilled water, and frozen at -80°C. The frozen insoluble material was thawed, washed twice in sterile PBS (Gibco, Grand Island, NY, USA) and mechanically homogenized (Polytron Kinematica, Luzern, Switzerland) and incubated with sterile-filtered dextranase (Sigma-Aldrich, St. Louis, MO, USA) at 37°C to digest the microcarrier beads. The solution was extensively washed with PBS to generate a final hECM material with a paste-like consistency and stored at 4°C until used in experiments.

Proteome characterization of CCM: Mass spectrometry analysis was performed by Proteome Sciences plc (UK) to identify and quantify proteins present in the CCM. The CCM samples underwent tryptic digest followed by liquid chromatography and mass spectroscopy followed by computational analysis to identify proteins present in the biological specimen.

Characterization of hECM: material was biochemically characterized as described elsewhere by measuring the collagen and sulfated glycosaminoglycan (sGAG) content. [34] The final hECM material was frozen at -80°C and lyophilized in a FreeZone 4.5 Liter benchtop freeze dry system (LabConco, Kansas City MO) to obtain dried material for collagen and sGAG analysis. The hydroxyproline content of lyophilized hECM was determined by first treating lyophilized hECM material with 6 N HCl and heating overnight at 115°C. The samples were neutralized to pH 7-8 with 1 N NaOH and then oxidized with Chloramine-T solution at room temperature followed by the addition of a perchloric acid solution. The samples were then reacted with p-dimethylaminobenzaldehyde (pDAB) and the colorimetric change was measured by at reading at 561 nm absorbance wavelength using a SpectraMax M3 plate reader (Molecular Devices, Sunnyvale, CA). The samples were fitted to a standard curve of 4-hydroxy-L-proline and the collagen content was calculated using a hydroxyproline concentration of 13.5% and expressed as mg collagen/mg dry weight of ECM. [35]

sGAG content of lyophilized hECM was performed by enzymatically digesting the material overnight at 60°C in a papain solution containing 0.1 M sodium phosphate, 10 mM EDTA solution, 5 mM cysteine solution, pH 6.5. The samples were reacted with the metachromatic dye dimethylmethylene blue (DMB) in a microtiter plate and read at an absorbance wavelength of 525 nm using a SpectraMax M3 plate reader (Molecular Devices, Sunnyvale, CA). The sample values were fitted to a standard curve of chondroitin sulfate from bovine cartilage and expressed as ug sGAG/mg dry weight of ECM. All chemicals for hydroxyproline and sGAG assays were from obtained from Sigma-Aldrich (St. Louis, MO).

Cell proliferation assays: In vitro studies were performed to measure the ability of a human embryonic-like CCM to support mesenchymal stem cell (MSC) proliferation while maintaining a stem phenotype. Human bone marrow MSCs were obtained from Cellular Engineering Technologies, Coralville, IA, Cat# HMSC-BM100 and cultured in monolayer with Hyclone Advance STEM medium (Hyclone Catalog SV30110.01) with growth supplements and 1% antibiotic/antimycotic additive. Cells were cultured for 3 days, passaged and then plated in T25 flasks. Control cultures received total growth medium while test cultures were fed with growth medium supplemented with 10% CCM. Cell counts were done at day 6 and 13.

Ex vivo rabbit disc study: An ex vivo thrombin-induced inflammation rabbit disc model was utilized to study the ability of CCM and hECM to reduced inflammatory factors and protease activity. New Zealand White Rabbit spines were isolated and cut into bone-disc-bone segments and cultured in nutrient media for 24 hours. Discs were then injected with 10ul of thrombin to induce a severe

inflammatory reaction. After 24 hours the AP and NP areas of the disc were injected with either 10 ul of phosphate buffered saline, hECM or CCM. Analysis of upregulated genes was assessed at 24 and 48 hours by qPCR.

In vivo rabbit disc study: New Zealand White rabbits [specific pathogen-free (SPF), 4-6 months-old, Western Oregon Rabbit Co. Philomath, Oregon] were used. Two to five days before the surgery, a pre-operative X-ray was taken as a baseline control under isoflurane anesthesia. Animals received Buprenex SR (0.1mg/kg) or Fentanyl Patch (12 mg) preoperatively as a preemptive analgesic. A dose of ketamine hydrochloride (35 mg/kg) xylazine (5 mg/kg) was given intramuscularly. Animals were intubated and maintained by isoflurane inhalation (induced at 2-3%, and maintained at 1-4%). The rabbits received 50 cc of fluids (Lactated Ringer's solution or NaCl) SQ while being prepped for surgery. Following prepping and draping, the lumbar IVDs were exposed through a posterolateral retroperitoneal approach by blunt dissection of the psoas muscle. The anterior surfaces of three consecutive lumbar IVDs (L2/3, L3/4 and L4/5) were exposed. Using an 18G needle with a stopper device that allows the needle to penetrate to a depth of 5 mm, the AF were punctured in the ventral aspect into the NP at the L2/3 and L4/5 levels. A titanium staple and a black silk suture were placed at L3/4 level as a reference point. The surgical wounds created were repaired in layers and the skin was closed using staples. During or after the surgery, an intra-operative X-ray was taken to confirm the level of puncture.

Two weeks after the initial surgery (annular puncture), a similar surgical procedure was made from the opposite side to avoid bleeding from the scar formed from the first operation. Once the surgically degenerating discs were confirmed by X-ray and visual inspection, test and control materials were intradiscally injected into the NP area with a microsyringe with 23G needle at both the L2/3 and L4/5 levels for each rabbit. At 2, 4, and 6 weeks after the initial annular puncture, an X-ray to measure IVD height was taken. X-rays were taken under isoflurane anesthesia.

Disc Height Index (DHI): All X-ray images were independently interpreted by an orthopedic researcher who was blinded to the study group and time point. Using digitized X-rays, measurements, including the vertebral body height and IVD height, were analyzed using the custom program for MATLAB software (Natick, MA). Data were transported to Excel software and the IVD height expressed as the disc height index (DHI = IVD height / adjacent IVD body height) based on the previously developed method. [35] The mean IVD height (DHI) was calculated by averaging the measurements obtained from the anterior, middle and posterior portions of the IVD and dividing that by the mean of the adjacent vertebral body heights. The average percent change in DHI of injected discs (both L2/3 and L4/5) was calculated for each postoperative disc as a ratio to its preoperative DHI (%DHI = postoperative DHI / preoperative DHI x100) and further normalized to the DHI of the non-punctured disc (L3/4): Normalized %DHI = (punctured %DHI/ non-punctured %DHI x100). (Figure 1) All radiographs were assessed by an observer blinded to this experiment.

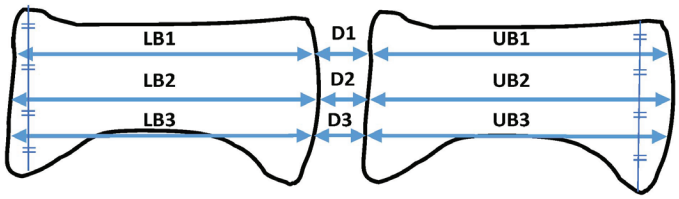

$$DHI = \frac{2(D1 + D2 + D3)}{(LB1 + LB2 + LB3) + (UB1 + UB2 + UB3)}$$

$$\%DHI = (\text{Post DHI}/\text{Pre DHI}) \times 100$$

$$\text{Normalized \%DHI} = \frac{\text{Target \%DHI}}{\text{L3/4 \%DHI}} \times 100$$

Figure 1: *Disc height index.*

7T MRI: MRI examinations were performed on all rabbit discs after sacrifice. MRI examinations on dissected specimens were performed on all the rabbits in the study using a BioSpec 70/30 USR (Bruker, ON). After sacrifice, the spinal columns, with surrounding soft tissue, were isolated and imaged. For anatomic images and Pfirrmann grading, T2-weighted images in the sagittal plane were obtained using the following settings: fast spin echo sequence with TR (time to repetition) = 3000 ms, TE (time to echo) = 100 ms, matrix=512x256, FOV=10, NEX=8, and slice thickness = 1 mm. Fifteen slices were obtained with a 0 mm gap. For semi-quantitative morphologic assessment, T2-weighted images were evaluated by two observers blinded to the experiment using the Pfirrmann classification based on changes in the degree and area of signal intensity from grades 1–5. The grades from the three observers were averaged to represent the grade for each disc. Histological processing was conducted to assess tissue quality of control, non-punctured, and treated disc tissue.

Histological analysis: Midsagittal sections (5 μm) of each experimental IVD from rabbits sacrificed at 6 weeks were stained with either hematoxylin and eosin or safranin-O. An observer blinded to this experiment analyzed the histologic sections and graded them using an established protocol (Table 1). [37]

I. Annulus Fibrosus:	
Grade:	
1.	Normal, pattern of fibrocartilage lamellae (U-shaped in the posterior aspect and slightly convex in the anterior aspect) without ruptured fibers and without a serpentine appearance anywhere within the annulus
2.	Ruptured or serpentined patterned fibers in less than 30% of the annulus
3.	Ruptured or serpentined patterned fibers in more than 30% of the annulus
II. Border between the annulus fibrosus and nucleus pulposus:	
Grade:	
1.	Normal
2.	Minimally interrupted
3.	Moderate/severe interruption
III. Cellularity of the nucleus pulposus:	
Grade:	
1.	Normal cellularity with large vacuoles in the gelatinous structure of the matrix
2.	Slight decrease in the number of cells and fewer vacuoles
3.	Moderate/severe decrease (>50%) in the number of cells and no vacuoles
IV. Matrix of the nucleus pulposus:	
Grade:	
1.	Normal gelatinous appearance
2.	Slight condensation of the extracellular matrix
3.	Moderate/severe condensation of the extracellular matrix

Histological grading scale based on four categories of degenerative changes with scores ranging from a normal disc with 4 points (1 point in each category) to a severely degenerated disc with 12 points (3 points in each category).

Table 1: *Histological Grading Scale.*

Results

CCM characterization: The mass spectrometry data showed a composition consisting of over 100 soluble extracellular matrix proteins and growth factors in the unconcentrated and 10x concentrated CCM (Table 2). Further studies demonstrated excellent lot to lot consistency.

Protein Description	Protein Description	Protein Description
Serum albumin	Triosephosphate isomerase	Isoform 2 of Neuroblastoma suppressor of tumorigenicity 1
Serotransferrin	Complement C1s subcomponent	Isoform M1 of Pyruvate kinase PKM
Isoform 15 of Fibronectin	Insulin-like growth factor-binding protein 6	Interleukin-8
Collagen alpha-2(I) chain	Collagen alpha-1-(III) chain	Transforming growth factor-beta-induced protein ig-h3
Tenascin	Nucleobindin-1	Isoform 3 of Latent-transforming growth factor beta-binding protein 1
Collagen alpha-1(I) chain	Peptidyl-prolyl cis-trans isomerase A	Isoform 2 of Fibulin-2
Vimentin	Stromelysin-1	Superoxide dismutase [Cu-Zn]
Follistatin-related protein 1	Isoform 2 of Mannan-binding lectin serine protease 1	C-X-C motif chemokine 5
Fibulin-1	Cystatin-C	Prostaglandin-H2 D-isomerase
Lumican	Isoform 2 of Latent-transforming growth factor beta-binding protein 4	Basement membrane-specific heparan sulfate proteoglycan core protein
Complement C3	Keratin, type I cytoskeletal 9	Filamin-A
Thrombospondin-1	Laminin subunit beta-1	Glyceraldehyde-3-phosphate dehydrogenase
Metalloproteinase inhibitor 1	Complement factor H	Isoform 2 of Insulin-like growth factor-binding protein 3
Insulin-like growth factor-binding protein 4	Chitinase-3-like protein 1	Trypsin-1

Collagen alpha-1-(VI) chain	Thymosin beta-4	Aldose reductase
Procollagen C-endopeptidase enhancer 1	Glia-derived nexin	Immunoglobulin superfamily containing leucine-rich repeat protein
Interstitial collagenase	Sulfhydryl oxidase 1	Retinoic acid receptor responder protein 2
Galectin-1	Peptidyl-prolyl cis-trans isomerase B	Cellular retinoic acid-binding protein 2
Growth-regulated alpha protein	Laminin subunit alpha-4	Galectin-3
72 kDa type IV collagenase	Fatty acid-binding protein, heart	Tropomyosin alpha-4 chain
Complement C1r subcomponent	Interleukin-6	Protein S100-A4
Isoform 2 of Fructose-bisphosphate aldolase A	Aminopeptidase N	Plasminogen activator inhibitor 1
Collagen alpha-3-(VI) chain	Isoform 3 of L-lactate dehydrogenase A chain	Actin, cytoplasmic 1
Isoform 4 of Tenascin-X	Beta-2-microglobulin	CD109 antigen
Isoform 2C2A of Collagen alpha-2-(VI) chain	Moesin	Phosphoglycerate kinase 1
Prelamin-A/C	Olfactomedin-like protein 3	Isoform 3 of Ecto-nucleotide pyrophosphatase/phosphodiesterase family member 2
Tetranectin	Peroxiredoxin-1	Isoform 2 of Glucose-6-phosphate isomerase
SPARC	Phosphoglycerate mutase 1	78 kDa glucose-regulated protein
Extracellular matrix protein 1	Apolipoprotein D	Extracellular superoxide dismutase [Cu-Zn]
Gelsolin	Keratin, type I cytoskeletal 10	Protein disulfide-isomerase A3
Laminin subunit gamma-1	Dickkopf-related protein 3	CD59 glycoprotein
Pigment epithelium-derived factor	14-3-3 protein zeta/delta	Metalloproteinase inhibitor 2
Keratin, type II cytoskeletal 1	Phosphatidylethanolamine-binding protein 1	Collagen alpha-1(XII) chain
EGF-containing fibulin-like extracellular matrix protein 1	Stanniocalcin-2	Plasminogen activator inhibitor 2
Insulin-like growth factor-binding protein 5	Isoform 2 of Procollagen-lysine,2-oxoglutarate 5-dioxygenase 1	Galectin-3-binding protein
Stanniocalcin-1	Fibrillin-1	Sushi, von Willebrand factor type A, EGF and pentraxin domain-containing protein 1
Insulin-like growth factor-binding protein 2	EMILIN-1	

Table 2: *Summary of major protein components of CCM as determined by mass spectrometric analysis.*

hECM characterization: The collagen and sGAG assay results confirmed lot-to-lot consistency of the material. Mass spec analysis showed that the hECM consists predominantly of human collagens I, II, III, and V, tenascin, vimentin, decorin, fibrillin, nexin, and basement membrane specific heparin sulfate proteoglycans.

Cell proliferation: Cell counts at day 7 after treatment with CCM supplemented media showed that the treated cultures had more than twice the number of MSCs. Enhanced proliferation of the treated cells continued to be seen past day 7 (Figure 2). The morphology of the cells was normal and treated cells reached confluence by day 13 whereas control cultures were less than 50% confluent at the same time.

Ex Vivo data: In hECM and CCM treated enzyme and protease activity was significantly decreased after only 24 hours, with levels being reduced to baseline or below($p<0.0001$). In addition, the treated IVDs demonstrated stimulation of the native disc cells to make new aggrecan ($p<0.0001$), a critical component in both the AF and NP of the (Figure 3) Given that the pathophysiology degeneration is associated with increased localized inflammation and enzymatic degradation and a breakdown of matrix proteins, having biomaterial that can reverse these localized effects has the potential of offering therapeutic benefit.

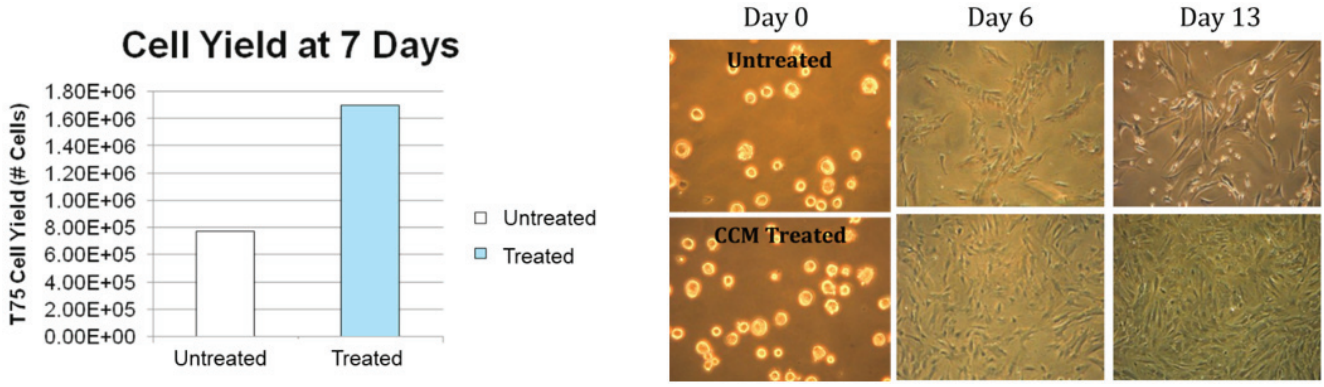

Figure 2: *CCM improves hMSC monolayer culture expansion.*

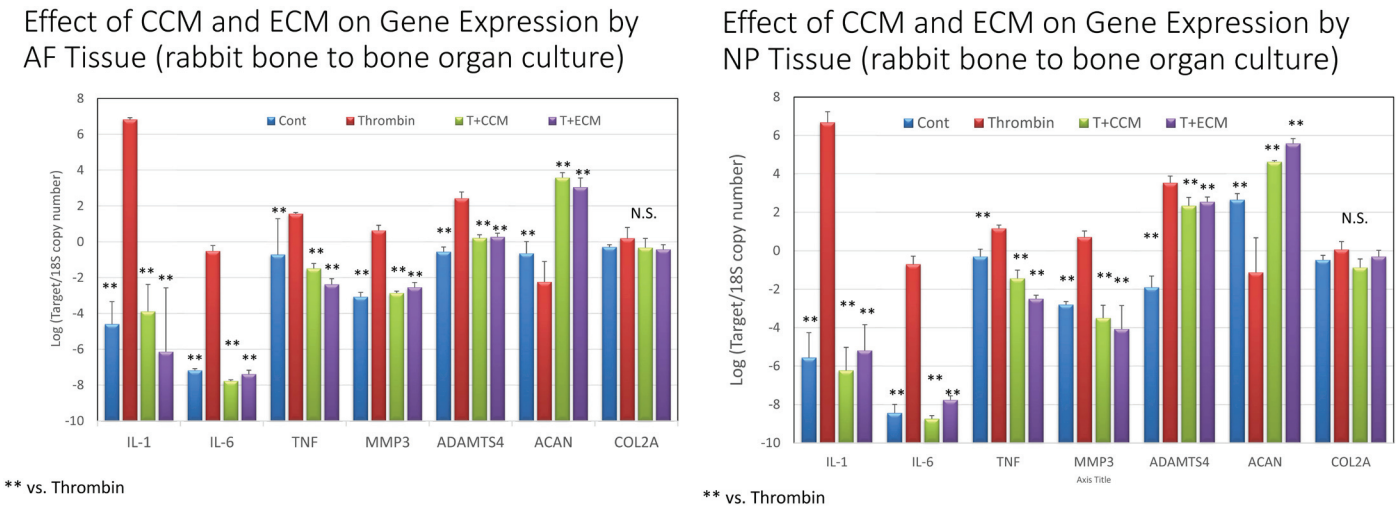

Figure 3: *Effect of CCM on Gene Expression by Spinal Disc Tissue (rabbit bone to bone organ culture).*

In Vivo Rabbit puncture results: Radiographic Images

The initial anular injury was induced in rabbit discs of 18 NZW rabbits; this procedure resulted in degenerative changes in the NP and AF. After 2 weeks, the rabbits were then injected with a vehicle control, hECM or CCM and followed up by X-ray. At 4 weeks after injection, both the hECM and CCM group showed wider disc space at the puncture level compared to the PBS control group (Figure 4).

Disc Height Index: The ECM and CCM group showed a tendency to be higher in disc height, compared to the PBS group, at the 4-week post-injection time point ($p=0.09$ and $p=0.10$, respectively, Figure 5).

MRI Analysis: Four weeks after PBS, hECM or CCM injection, L3/4 control discs in all groups did not exhibit disc degeneration (Figure 5). The signal intensity of NP in the CCM and ECM groups was stronger than in the PBS group. (Figure 6, center and right panel).

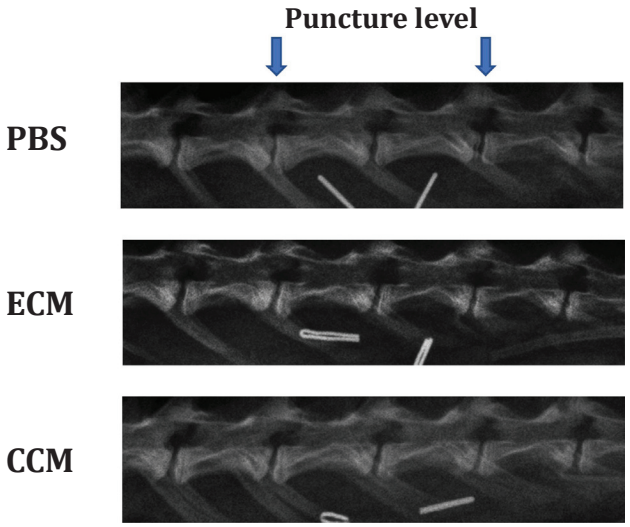

Figure 4: *X-ray images 4 weeks post-injection of PBS (control), hECM and CCM.*

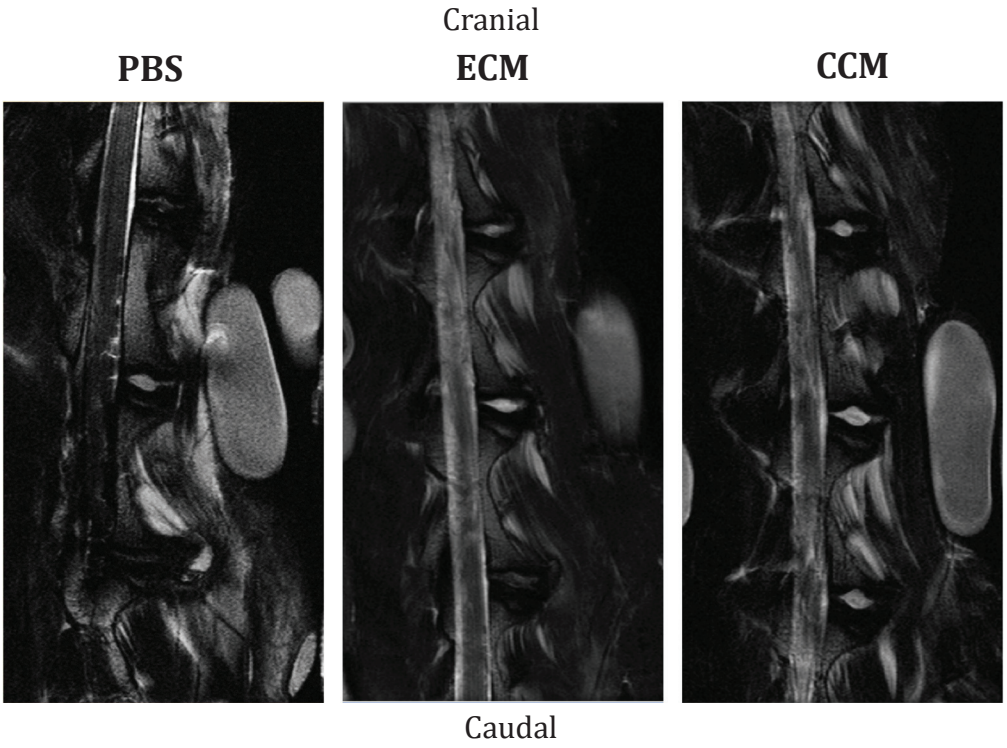

Figure 5: *7T MRI images 4 weeks post-injection of PBS (control), hECM and CCM.*

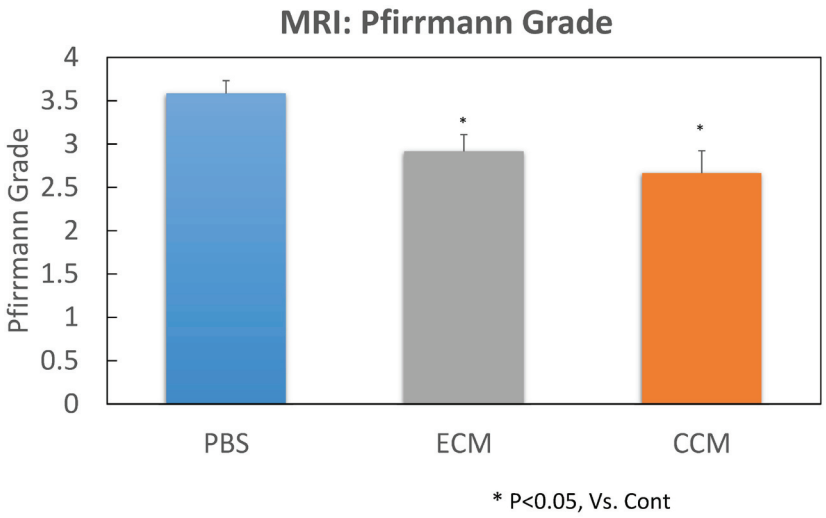

Figure 6: *Pfirrmann grading of PBS (control), hECM and CCM treated discs at 4 weeks.*

Pfirrmann grade analysis: After 4 weeks following treatment, there was a significant difference between PBS vs. treatment groups in Pfirrmann Grading ($p<0.05$, Figure 7).

Histological analysis: Total histological scores of all puncture discs were significantly higher than that of the non-puncture control discs (L3/4). The injection of PBS did not show a significant effect on the overall histological score of disc degeneration 4 weeks after injection. The score in the CCM and hECM groups were significantly higher than in the PBS group (both $P<0.01$). The NP in CCM showed the maintenance of the original structure and the cells in the AF show round-shape chondrocytic changes. In the hECM group, a similar trend was seen.

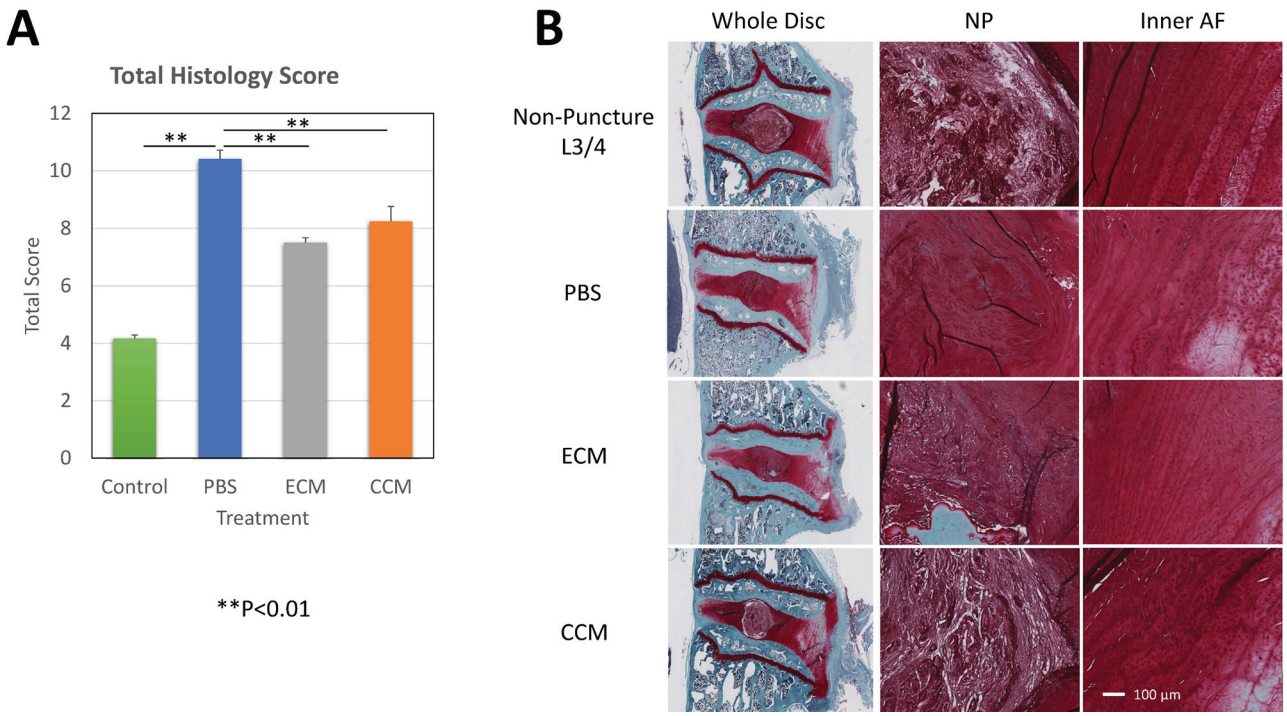

Figure 7: *(A) The histology scores in the ECM and CCM groups were significantly lower than those of the PBS group (both p<0.01). (B) The NP in CCM showed the maintenance of the original structure and the cells in the AF show round-shape chondrocytic changes. In the ECM group, a similar trend was seen.*

Discussion

The results from this study support further investigation into using the bioengineered biomaterials as a treatment to regenerate new functional tissue in intervertebral disc degeneration which was either caused by a recent traumatic accident or damage due to inflammatory cytokines and matrix degradation by local protease activity. A treatment with anti-inflammatory and regenerative properties, like those seen with both CCM and hECM, has the potential to be utilized at the time of IVD injury or in conjunction with inflammation induced IDD to heal/regenerate hyaline cartilage and fibrous tissue and prevent further matrix degeneration, resulting in more rapid and full recovery. In addition to reducing/eliminating harmful protease and inflammatory cytokine activity both biomaterials stimulate native cells in the disc to result in the maintenance of disc tissue, formation of new matrix and partially restored disc height in as little as 4 weeks. Given that the CCM demonstrated the most significant regeneration of tissue and is easily injected into the confined area of a damage disc, future long-term animal studies and clinical studies will focus on the use of the soluble material for disc repair and regeneration.

References

1. G.B.D. 2016 D. and I.II and P Collaborators, (2017). Global, regional, and national incidence, prevalence, and years lived with disability for 328 diseases and injuries for 195 countries. 1190-2016: a systemic analysis of the global burden of Disease study. 2016. Lancet 390:1211-1259.
2. Katz, JN. (2006). Lumbar disc disorders and lower back pain: socioeconomic factors and consequences. J Bone Joint Surg Am.: 88:2-24.
3. Antonious J, Steffen T, et al. (1996). The human lumbar intervertebral disc: evidence for changes in the biosynthesis and denaturation of the extracellular matrix with growth, maturation, ageing, and degeneration. J Clin Invest 98: 996-1003.
4. Roberts S, Caterson B, Menage J, Evans EH, Jaffray DC, Eisenstein SM. (2000). Metrix metalloproteases and aggrecanase: their role in disorders of the human intervertebral disc. Spine 25: 3005-3013.

5. Le Maitre CL, Freemont AJ, Hoyland JA. (2004). Localization of degradative enzymes and their inhibitors in the degenerate human intervertebral disc. J Pathol 204: 47-54.
6. Le Maitre CL, Freeemont AJ, Hoyland JA. (2005). The role of interleukin-1 in the pathogenesis of human intervertebral disc degeneration. Arthritis Res Ther 7: 732-745.
7. Wuertz K, No N, Kletsas D, Boos N. (2012). Inflammation and catabolic signaling in intervertebral discs: the roles of NF-kB and MAP kinases. Eur Cell Mater 23: 1103-119.
8. Shamji MF, Setton LA, Jarvis W, et al. (2010). Proinflammatory cytokine expression profile in degenerated and herniated human intervertebral disc tissues. Arthitis Rheum 62:1974-1982.
9. Burke JG, Watson RWG, McCormack D, Dowling FE, Walsh MG, Fitzpartrick JM. (2002). Intervertebral discs which cause low back pain secrete high levels of proinflammatory mediators, J Bone Joint Surg Br 84: 196-201.
10. Kang JD, Georgescu HI, McIntyre-Larkin I, Stefanovic-Racic M, Evans CH. (1995). Herniated cervical intervertebral discs spontaneously produce matrix metalloproteases, nitric oxide, interleukin-6, and prostaglandin E2. Spine 20: 2372-2378.
11. Oldmarker K, Larsson K. (2005). Tumor necrosis factor alpha and nucleus-pulposus-induced nerve root injury: a study in surgical specimen and autopsy controls. Spine 30: 44-53.
12. Igarashi T, Kikuchi S, Shubayev V, Myers RR, (2000). Exogenous tumor necrosis factor α mimics nucleus pulposus-induced neuropathy. Molecular, histologic, and behavioral comparisons in rats. Spine 25: 2975-2980.
13. Aoki Y, Rydevik B, Kikuchi S, Oldmarker K. (2002). Local application of disc-related cytokines on spinal nerve roots. Spine 27: 1614-1617.
14. Brisby H. Byrod G, Oldmarker K, Miller VM, Aoki Y, Rydevik B. (2000). Nitric oxide as a mediator of nucleus pulposus-induced effects on spinal nerve roots. J Orthop Res 18: 815-820.
15. Keshari KR, Lotz JC, Link TM, Hu S, Majumdar S, Kurhanewicz J. (2008). Lactic acid and proteoglycans as metabolic markers fir discogenic back pain. Spine 33: 312-317.
16. Hwang SW, Oh U. (2007). Current concepts of noviception: nociceptive molecular sensors in sensory neurons. Curr Opin Anaesthesiol 20: 427-434.
17. Weiler C, Nerlich AG, Bachmeier BE, Boos N. (2005). Expression and distribution of tumor necrosis factor alpha in human lumbar intervertebral discs: a study in surgical specimen and autopsy controls. Spine 30: 44-53.
18. Thompson JP, Pearce RH, Schechter MT, Adams ME, Tsang IK, Bishop PB. (1990). Preliminary evaluation of a scheme for grading the gross morphology of the human intervertebral disc. Spine 15: 411-415.
19. Boos N, Weissbach S, Rohrbach H, Weiler C, Spratt KF, Nerlich AG. (2002). Classification of age-related changes in lumbar intervertebral discs: Spine 27: 2631-2644.
20. Ebara S, Iatridis JC, Setton LA, Foster RJ, Mow VC, Weidenbaum M. (1996). Tensile properties of non-degenerative human lumbar annulus fibrosus. Spine 21: 452-461.
21. Michael T. Bayliss and Brian Johnstone. (1992). The lumbar spine and back pain, chapter 7. Biochemistry of the intervertebral disc, pp 111-127. Churchill Livingstone, 4th edition.
22. Heather A Horner, Sally Roberts, Robert C Bielby, Janis Menage, Helan Evans, and Jill P.G. Urban. (2002). Cells from different regions of the intervertebral disc, effect of culture system on matrix expression and cell phenotype. Spine, 10: 1018-1028.
23. Susan R. S. Bibby, Deboray A Jones, Robert B. Lee, Jing Yu, and Jill P.G. Urban. (2001). The pathophysiology of the intervertebral disc. Joint Bone Spine, 68: 537-542.
24. Jill P. G. Urban, Stanton Smith, and Jeremy Fairbank. (2004). Nutrition of the intervertebral disc. Spine 29 (23): 2700-2709.
25. T. Aigner, L. Hambach, S. Sder, U Schltzer-Schrehardt, and E. Pschl. (2002). The c5 domain of col6a3 is cleaved off from the co16 fibrils immediately after secretion. Biochemical and Bioplhysical Research Communications, 290: 743-748.
26. Degen KE, Gourdie RG. (2012). Embryonic wound healing: a primer for engineering novel therapies for tissue repair. Birth Defect Res. 96: 258-270.
27. Al-Qattan MM, Posnick JC, Lin KY, and Thorner P. (1993). Fetal tendon healing: development of an experimental model. Plast Reconstr Surg. 92: 1155.
28. Adzick N, Lorenz P. (1994). Cells, Matrix, Growth Factors, and the Surgeon. Ann Surg. 220 (1): 10-18.
29. Decker RS, Um HB, Dyment NA, Cottingham N, Usami Y, Enomoto-Iwamoto M, Kronenberg MS, Maye P, Rowe DW, Koyama E, et al. (2017). Cell origin, volume and arrangement are drivers of articular cartilage formation, morphogenesis and response to injury in mouse limbs. Dev Biol. 426:56-68.
30. Jenner F, Ijpma A, Cleary M, Heijsman D, Narcisi R, van der Spek PJ, Kremer A, van Weeren PR, Brama P, and van Osch GJVM. (2014). Diiferential gene expression of the intermediate and outer interzone layers of developing articular cartilage in murine embryos. Stem Cells Dev 23: 1883-1898.

31. Pinney E, Zimber MP, Schenone A, Montes-Camacho M, Naughton GK. (2011). Human Embryonic-like ECM (hECM) stimulates proiiferation and differentiation in stem cells while killing cancer calls. Inter J of Stem Cells. 4: 70-75.
32. Page RL, Ambady S, Holmes WF, Vilner L, Kole D, Kashpur O, Huntress V, Vojtic I, Whitton H, Dominko T. (2009). Induction of Sem Cell Gene Expression in Adult Human Fibroblasts without Transgenes. Cloning and Stem Cells. 11(3).
33. Zhou Y, Zimber M, Yuan H, Naughton GK, Fernan R, Li WJ. (2016). Effects of Human Fibroblast-Derived Extracellular Matrix on Mesenchymal Stem Cells. Stem Cell Reviews and Reports, 12(5), 560–572.
34. Neuman, R. E., Logan, M. A. (1950). The determination of collagen and elastin in tissues. J Bio Chem 186: 549.
35. Masuda K, Aota Y, Muehleman C, Imai Y, Okuma M, Thonar EJ, Andersson GB, An HS. (2005). A novel rabbit model of mild, reproducible disc degeneration by an anulus needle puncture: correlation between the degree of disc injury and radiological and histological appearances of disc degeneration. Spine (Phila Pa 1976). 30(1):5-14.
36. Miyazaki S, Diwan AD, Kato K, Cheng K, Bae WC, Sun Y, Yamada J, Muehleman C, Lenz ME, Inoue N, Sah RL, Kawakami M, Masuda K. (2018). ISSLS PRIZE IN BASIC SCIENCE 2018: Growth differentiation factor-6 attenuated pro-inflammatory molecular changes in the rabbit anular-puncture model and degenerated disc-induced pain generation in the rat xenograft radiculopathy model. Eur Spine J. 27(4):739-51.
37. Chujo T, An HS, Akeda K, Miyamoto K, Muehleman C, Attawia M, Andersson G, Masuda K. (2006). Effects of growth differentiation factor-5 on the intervertebral disc--in vitro bovine study and in vivo rabbit disc degeneration model study. Spine (Phila Pa 1976). 31(25): 2909-17.